remote sensing

MDPI

Article

# Assessing Groundwater Sustainability in the Arabian Peninsula and Its Impact on Gravity Fields through Gravity Recovery and Climate Experiment Measurements

**Hussein A. Mohasseb [1,2], Wenbin Shen [1,2,*], Hussein A. Abd-Elmotaal [3] and Jiashuang Jiao [2,4]**

1 State Key Laboratory of Information Engineering in Surveying, Mapping and Remote Sensing (LIESMARS), Wuhan University, Wuhan 430079, China; hussein985@whu.edu.cn
2 School of Geodesy and Geomatics, Wuhan University, Wuhan 430079, China; jiashuang.jiao@whu.edu.cn
3 Civil Engineering Department, Faculty of Engineering, Minia University, Minia 61111, Egypt; hussein.abdelmotaal@gmail.com
4 Wuhan Gravitation and Solid Earth Tides National Observation and Research Station, Wuhan 430071, China
* Correspondence: wbshen@sgg.whu.edu.cn; Tel.: +86-27-6877-1539

**Abstract:** This study addresses the imperative to comprehend gravity shifts resulting from groundwater storage (GWS) variations in the Arabian Peninsula. Despite the critical importance of water resource sustainability and its relationship with gravity, limited research emphasizes the need for expanded exploration. The investigation explores the impact of GWS extraction on the gravity field, utilizing Gravity Recovery and Climate Experiment (GRACE) and Global Land Data Assimilation System (GLDAS) data in addition to validation using the WaterGAP Global Hydrology Model (WGHM). Spanning April 2002 to June 2023, this study predicts GWS trends over the next decade using the Seasonal Autoregressive Integrated Moving Average (SARIMA) model. The comprehensive time-series analysis reveals a significant GRACE-derived groundwater storage (GWS) trend of approximately $-4.90 \pm 0.32$ mm/year during the study period. This trend has a notable impact on the gravity anomaly (GA) values, as observed through the decomposition analysis. The projected GWS indicates a depletion rate of 14.51 km$^3$/year over the next decade. The correlation between GWS and GA is substantial at 0.80, while the GA and rainfall correlation is negligible due to low precipitation rates. Employing multiple linear regression explains 80.61% of the variance in gravity anomaly due to GWS, precipitation, and evapotranspiration. This study investigates climate change factors—precipitation, temperature, and evapotranspiration—providing a holistic understanding of the forces shaping GWS variations. Precipitation and evapotranspiration exhibit nearly equal values, limiting GWS replenishment opportunities. This research holds significance in studying extensive GWS withdrawal in the Arabian Peninsula, particularly concerning crust mass stability.

**Keywords:** GRACE; gravity anomaly; groundwater; TWS; SARIMA; Arabian Peninsula

check for updates

**Citation:** Mohasseb, H.A.; Shen, W.; Abd-Elmotaal, H.A.; Jiao, J. Assessing Groundwater Sustainability in the Arabian Peninsula and Its Impact on Gravity Fields through Gravity Recovery and Climate Experiment Measurements. *Remote Sens.* **2024**, *16*, 1381. https://doi.org/10.3390/rs16081381

Academic Editors: Ehsan Forootan, Liming He, Natthachet Tangdamrongsub and Pavel G. Ditmar

Received: 22 February 2024
Revised: 27 March 2024
Accepted: 11 April 2024
Published: 13 April 2024



## 1. Introduction

In arid regions such as the Arabian Peninsula, where water scarcity poses a formidable challenge, groundwater emerges as a vital and often irreplaceable resource that is crucial for sustaining life, agriculture, and economic development [1,2]. The Arabian Peninsula, encompassing countries such as Saudi Arabia, Yemen, Oman, the United Arab Emirates, Bahrain, Kuwait, and Qatar, is characterized by its arid climate and limited freshwater resources [3]. The significance of groundwater in these arid landscapes cannot be overstated, as it serves as a primary source of water for both domestic and agricultural needs [4]. With limited surface water features such as rivers and reservoirs, the Arabian Peninsula heavily relies on groundwater to meet the escalating demands of a growing population and expanding agricultural practices [5]. Groundwater plays a pivotal role in sustaining life and supporting various sectors in this predominantly desert region [6,7]. With sparse surface water features, these nations heavily rely on underground aquifers to meet their water needs for agriculture, industry, and domestic consumption [8]. However, the groundwater situation in the Arabian Peninsula faces challenges such as over-extraction, declining water levels, and the threat of salinity intrusion. Rapid population growth, urbanization, and increased agricultural demands contribute to the strain on these precious water resources [9–11]. The over-extraction of groundwater and declining water levels in the Arabian Peninsula have profound effects on the Earth's gravitational field, which can be observed through techniques such as satellite-based measurements [12]. Excessive withdrawal of groundwater alters the mass distribution beneath the Earth's surface, leading to a reduction in terrestrial water storage. This decline in water mass contributes to changes in the gravity field (Figure 1) [13,14].

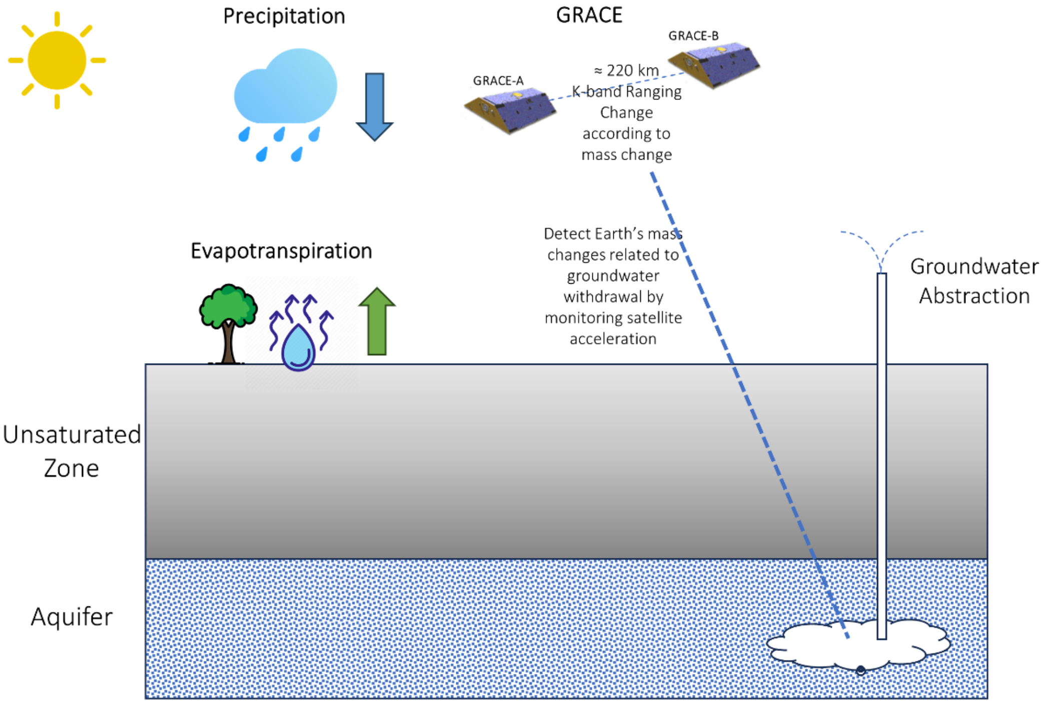


**Figure 1.** The schematic of the hydrological setting in the Arabian Peninsula in addition to GRACE satellite (Authers calculations).

In the Arabian Peninsula, the dependence on groundwater for renewable water resources is pronounced. Kuwait relies entirely on groundwater, constituting 100% of its renewable water resources, while Bahrain heavily depends on it, accounting for 96.6% of its water supply [15]. Water withdrawal in the Arabian Peninsula is predominantly driven by agriculture, with a significant contribution to the overall water demand [16,17]. Non-conventional water sources play a vital role in addressing water scarcity in the Arabian Peninsula. Bahrain and Kuwait, in particular, heavily rely on non-conventional sources for over 90% of their water resources [18,19]. Desalinated water is a key contributor, with Saudi Arabia, the United Arab Emirates, and Kuwait collectively using 931 million $m^3$/year. The total annual water withdrawal for Arabian Peninsula countries is 271.5 $km^3$, which is around 7% of world withdrawals [20]. About 84% of inventoried withdrawals are from agriculture, which is higher than the value for global agricultural water withdrawal (70%) [16]. In Saudi Arabia, Oman, and Yemen, agricultural withdrawal accounts for more than 85% of the total water withdrawal, while in Bahrain, Kuwait, and Qatar, it represents less than 60% [21].

Monitoring groundwater on a large scale through well networks is both challenging and expensive due to issues such as temporal data inconsistencies, uneven well distribution, and complex subsurface properties, compounded by restricted data access [22,23]. Seeking alternatives since the 1970s, scientists introduced the National Aeronautics and Space Administration's (NASA) twin Gravity Recovery and Climate Experiment (GRACE) mission in March 2002 [24,25]. GRACE was followed by GRACE-FO in mid-2018 after 15 years of unprecedented observation by GRACE. GRACE and GRACE-FO employ K-Band microwave technology to directly measure groundwater changes by estimating variations in Earth's gravity field, providing a distinct advantage over traditional monitoring methods [26–28]. The use of GRACE-derived groundwater storage (GWS) has proven more effective in representing in situ groundwater levels, as demonstrated by various studies quantifying groundwater variability through GRACE gravity measurements [26,29–33]. Despite the challenges, the application of satellite-based technologies like NASA's GRACE mission has become indispensable for directly measuring global groundwater changes, with a notable focus on addressing GWS changes in the intricate hydrogeological setting of the Arabian Peninsula [34–36].

In their investigation within the Abu Dhabi Emirate, UAE, Alghafli, et al. [37] employed GRACE satellite measurements to scrutinize declining groundwater levels attributed to agricultural expansion and urban development. Their research underscores GRACE data's effectiveness in estimating groundwater recharge, emphasizing the need for regulations to ensure sustainable groundwater development in arid regions, revealing a notable agreement ($R^2$ = 0.91) between in situ and GRACE-derived recharge estimates. Mohamed, et al. [35] utilized advanced geophysical and remote sensing techniques, integrating GRACE data with land surface model outputs and rainfall data, to analyze spatiotemporal mass fluctuations induced by groundwater changes over the Southern Arabian Peninsula. Their findings showcase average annual precipitation rates ranging from 54.6 to 117 mm/year and negative trends in average ΔTWS values, highlighting the Rub El Khali region's lower precipitation rates and higher negative groundwater storage trends compared to the southern and eastern regions.

Addressing the Saq transboundary aquifer system in the arid Arabian Peninsula, Fallatah, et al. [38] analyzed GRACE data, revealing significant depletion rates in TWS (−9.05 mm/year) and GWS (−6.52 mm/year), attributed to both climate and increased groundwater extraction for irrigation. Their integrated approach aims to inform sustainable management of the Saq aquifer system and address water resource challenges in the region. Employing the global hydrological model WaterGAP, Döll, et al. [39] quantified groundwater depletion (GWD) in the Arabian Peninsula and globally using GRACE data. The results indicate that in Arabian Peninsula countries like Saudi Arabia, at least 30% of abstracted groundwater is sourced from nonrenewable reserves, contributing to a significant global GWD increase estimated to have more than doubled from an average of 56 $km^3$/year to 113 $km^3$/year between 1960 and 2000 and 2000 and 2009.

Focusing on Saudi Arabia's water shortage, Mohamed, et al. [40] integrated GRACE data with other relevant information, revealing a decline in groundwater storage with an average depletion rate of $-5.33 \pm 0.22$ mm/year during the study period (April 2002 to July 2016), driven by factors such as heavy groundwater extraction and drought. Their approach is considered informative and cost-effective for efficiently assessing groundwater resource variability in large areas. Addressing groundwater quality in Saudi Arabia, Fallatah [41] utilized GRACE data to quantify groundwater storage depletion (GWS) from April 2002 to April 2016. Findings reveal a GRACE-derived GWS depletion rate of $-2 \pm 0.13$ $km^3$/year, with water quality assessments indicating high total dissolved solids (TDS) in domestic wells from the Arabian Shield, rendering the water unsuitable for drinking. The integrated approach, combining GRACE data with geological and hydrological information, aims to inform sustainable water resource management in the arid Arabian Peninsula.

Despite the critical importance of GWS in arid regions like the Arabian Peninsula, there is a noticeable shortage of comprehensive studies investigating the associated changes in gravity. In their study, Agarwal, et al. [42] employed GRACE and InSAR data to explore the relationship between groundwater levels, precipitation, and Earth's gravity anomaly (GA). Using linear regression models, they found that groundwater recharge resulted in surface uplift, while large groundwater extraction led to land subsidence. The estimated groundwater loss from GRACE data was approximately 9.003 million cubic meters, and land movement values ranged from −6 to +6 mm/year. Understanding and quantifying the alterations in gravity resulting from GWS variations are essential for assessing water resource sustainability, yet research in this area remains limited, highlighting the need for further exploration and monitoring in the region. This pioneering study is the first to explore the impact of GWS extraction on the gravity field in the Arabian Peninsula, shedding light on the complex interplay between human activities and Earth's gravitational dynamics. Additionally, the research investigates the influence of climate change factors, such as rainfall, temperature, and evapotranspiration, providing a comprehensive understanding of the multifaceted forces shaping GWS variations and their repercussions on the gravity field. This study pioneers the prediction of GWS trends over the next decade. Using the SARIMA technique, drawing insights from comprehensive historical data spanning from April 2002 to June 2023. By leveraging the GRACE and hydrological models' datasets, this research aims to provide valuable foresight into the future trajectory of GWS.

## 2. Materials and Methods

### *2.1. Study Area*

The Arabian Peninsula (AP) is situated in southwest Asia and is bordered to the west by the Red Sea, the south by the Arabian Sea, and the northeast by the Persian Gulf (refer to Figure 2a) [43]. The region boasts a diverse landscape encompassing arid deserts, mountain ranges, and coastal plains. Spanning an area of about 3.103 million km$^2$, it covers approximately 4.7% of the world's total land area and accommodates 4.25% of the global population (refer to Table 1 and Figure 2a,b). We recognize the limitations of GRACE data in capturing small-scale hydrological processes. While GRACE offers valuable insights at a large scale, its spatial resolution and sensitivity to localized variations present challenges. However, the AP area exceeds the GRACE spatial resolution, approximately 160,000 km$^2$. Despite this vastness, the Arabian Peninsula's water resources constitute only about 1.1% of the world's total renewable water resources [44].

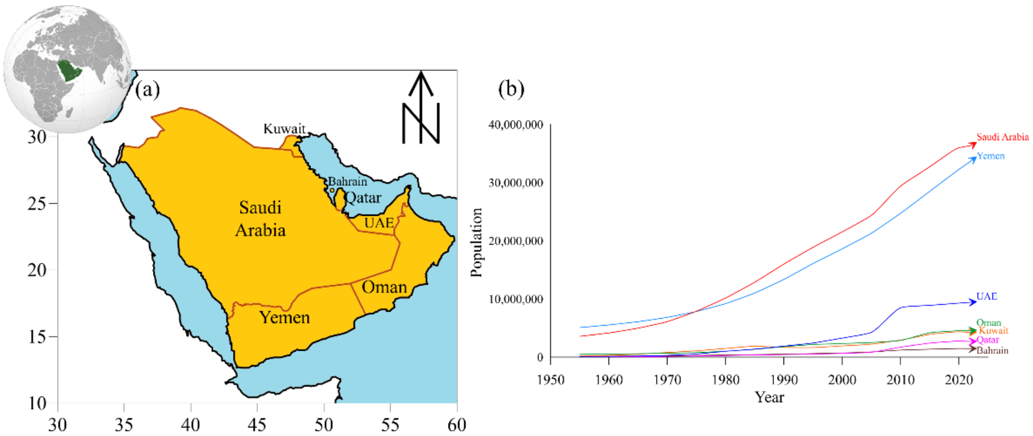


**Figure 2.** (**a**) The deep yellow region is the geographical location of the Arabian Peninsula and its seven countries, and (**b**) the time-series depicting population growth from 1955 to 2023, with Saudi Arabia in red, Yemen in light blue, the United Arab Emirates in blue, Oman in green, Kuwait in orange, Qatar in pink, and Bahrain in brown (authors' calculation).

**Table 1.** Information on the area and population of countries within the AP.

| Country | Area ($km^2$) | Population 2023 (Million) |
|---|---|---|
| Bahrain | 652 | 1.491 |
| Kuwait | 17,818 | 4.328 |
| Oman | 212,460 | 4.676 |
| Qatar | 11,610 | 2.726 |
| Saudi Arabia | 2,149,690 | 37.189 |
| UAE | 83,600 | 9511 |
| Yemen | 555,001 | 34,800 |
| Total | 3,030,831 | 94.721 |

In spite of the high population growth and water demand (Figure 2b), renewable water availability is less than 100 $m^3$ per person-year in places like Kuwait, Bahrain, and Qatar. The groundwater aquifers cover two-thirds of Saudi Arabia and some of them extend into Kuwait, Bahrain, Qatar, the United Arab Emirates, Oman, and Yemen [45]. Yemen already has one of the lowest annual per capita water shares in the world, estimated at 125 cubic meters [46].

The AP consists of several countries, including Saudi Arabia, the largest both in land area and population, the United Arab Emirates to the southeast, Yemen in the southwestern corner, mountainous Oman to the southeast, the island group of Bahrain in the Arabian Gulf, West Asian country Qatar occupying the Qatar Peninsula on the northeastern coast, and Kuwait located at the northern edge of the Eastern AP, situated at the tip of the Persian Gulf and bordering Iraq to the north and Saudi Arabia to the south [47].

This region is distinguished by its distinctive topography, which encompasses deserts and lofty mountains. It features a dry climate, particularly with soaring temperatures in the summer. The vast expanse exhibits diverse climate zones, with the northern part classified as subtropical (north of 20°N) and the southern part characterized by a tropical (monsoonal) climate type. According to Figure 3, the AP region has an arid climate with less than 96 mm per year average rainfall (about 7.99 mm/month) (Figure 3b) and an evaporation rate of about 81 mm per year (6.74 mm/month) (Figure 3c) because of the average temperature of about 26.5 °C (Figure 3a).

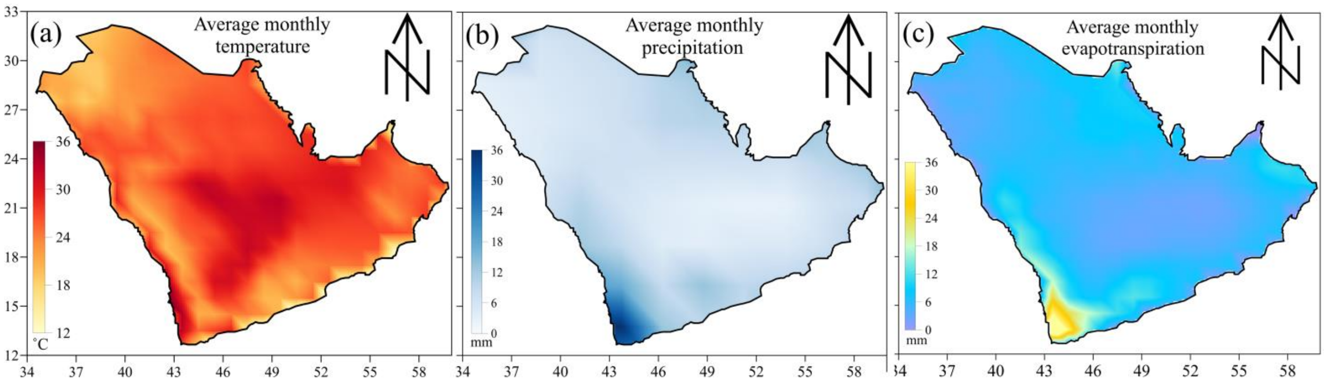


**Figure 3.** The climate factors of the Arabian Peninsula throughout the study period from April 2002 to June 2023, showcasing (**a**) the average monthly temperature using Global Historical Climatology Network version 2 and the Climate Anomaly Monitoring System (GHCN-CAMS), (**b**) the average monthly precipitation using from the Global Precipitation Climatology Project (GPCP), and (**c**) the average monthly evapotranspiration using Global Land Data Assimilation System (GLDAS) (authors' calculation).

## 2.2. Data Used

### 2.2.1. GRACE Data

The GRACE-mission was a collaborative effort between NASA and the German Aerospace Center (DLR) that took flight in March 2002, concluding its operations in June 2017 [24]. With over 15 years of successful data collection and analysis, NASA and the German Research Centre for Geosciences (GFZ) decided to initiate the GRACE-FO mission in May 2018. The primary aim of these missions was to meticulously measure Earth's gravity field and enhance our understanding of its water distribution, spanning across land, ice, and oceans [48]. The primary data acquired from the GRACE/GRACE-FO missions comes in two forms: spherical harmonic coefficients (SHCs) and mass concentration blocks (mascon) data. GRACE/GRACE-FO mascons data are presented as an equivalent water thickness at about monthly intervals (in centimeters), which represent the TWS [49]. The gridded GRACE data range from 0.25° for the University of Texas Center for Space Research (CSR) to 0.5° for Jet Propulsion Laboratory (JPL) data centers [50]. For the purposes of this study, for GWS, we focused on mascon data from release-06.2, which were obtained from the two processing centers: CSR and JPL. While for GA, we focused on SHC data from release-06, which were obtained from the CSR processing center. We made some corrections to the GRACE and GFO data. Due to the low accuracy of the original value, $C_{20}$ and $C_{30}$ coefficients are replaced by its value in satellite laser-ranging SLR [51]. Furthermore, due to geocentric motion, degree-1 coefficients were corrected using Swenson, et al. [52] results. Finally, we removed correlated errors using the approach described by Swenson and Wahr [53].

These datasets, spanning from April 2002 to June 2023, were subject to a bilinear interpolation process where CSR GRACE Mascon products were upscaled to a resolution of 0.5 degrees to match that of the JPL GRACE product. In this analysis, the averaged data were utilized from these datasets, a practice known to enhance accuracy. To address gaps in the data, such as missing monthly measurements and the 11-month transition period between GRACE and GRACE-FO, the monsoon linear regression analysis was employed, providing a comprehensive and continuous dataset for this study [30].

### 2.2.2. Hydrological Models

The Global Land Data Assimilation System (GLDAS) is assimilating observational data products acquired from satellite and ground-based sources. This process involves the use of advanced LSM techniques and data-assimilation methods to create optimal representations of land surface conditions and fluxes [54]. As a result, the GLDAS project has generated an extensive repository of globally modeled and observed surface meteorological data, parameter maps, and outputs. This study employed the GLDAS-Noah L4-monthly 1.0 × 1.0-degree Product V2.1 [55,56]. This specific dataset serves as a valuable resource to estimate the GWS variations.

The WaterGAP Hydrological Model (WGHM) data, characterized by a spatial resolution of 0.5° by 0.5° (approximately 55 km by 55 km at the equator) and covering a period from Jan 2003 to December 2019, is a valuable tool for analyzing GWS dynamics [57]. Originating from the WaterGAP 2 model, which computes human water use and net abstractions from groundwater (GW) and surface water (SW) in various global sectors, the resulting abstractions are incorporated into the WGHM [39,57–59]. This global hydrological model operates with daily time steps, simulating intricate flows among different water storage compartments such as canopy, snow, soil, GWS, lakes, man-made reservoirs, wetlands, and rivers.

### 2.2.3. Meteorological Data

Precipitation (*Pr*) is a pivotal meteorological element that plays a significant role in the circulation of water and is closely associated with both flooding and drought events. In this study of GWS variations, we incorporated *Pr* data obtained from the Global Precipitation Climatology Project (GPCP) [60,61]. To further enhance our analysis, we integrated data from two extensive sources of station observations, namely the Global Historical Climatology Network version 2 (GHCN) and the Climate Anomaly Monitoring System (CAMS). This combined dataset was instrumental in estimating the monthly global surface air temperature dataset, offering insights into temperature variations on a global scale. Notably, these datasets possess a spatial resolution of 0.5 degrees by 0.5 degrees, ensuring a comprehensive and detailed perspective for our research.

## 3. Methodology

In this study, we focus on three directions: GWS estimation, gravity change, and climate factors affecting GWS change. Figure 4 shows the flowchart of the methodology used in this study.

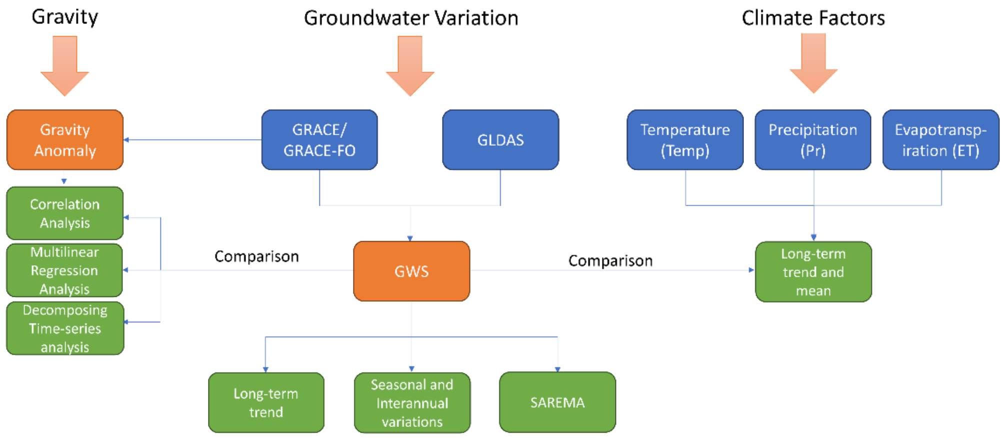


**Figure 4.** The flowchart of the methodology used in this study (authors' calculation).

### 3.1. GWS Estimation

The approach for estimating GWS in the AP employs a comprehensive strategy that integrates GRACE mascon data with GLDAS Noah model data pertaining to soil moisture. The GRACE mascon data capture variations in Earth's gravitational field, facilitating the evaluation of alterations in water storage. The processed mascon data provide equivalent water height anomalies (ΔEWH), offering insights into fluctuations in TWS [26]. Concurrently, the inclusion of GLDAS Noah data, which incorporate information on soil moisture, enhances the analytical framework. The GWS estimation entails the integration of GRACE mascon and GLDAS Noah data through a specified formula (Equation (1)).

$$\Delta \text{GWS} = \Delta \text{TWS} - (\Delta \text{SMS} + \Delta \text{SWS} + \Delta \text{SWE} + \Delta \text{CWS}) \quad (1)$$

This equation calculates the change in groundwater storage (ΔGWS) by subtracting changes in soil moisture (ΔSM), surface water (ΔSWS), snow water equivalent (ΔSWE), and canopy water (ΔCWS) from TWS. Importantly, in semi-arid regions like the AP, where gravimetric fluctuations in surface water storage are negligible, contributions from ΔSWS are considered insignificant [62]. Furthermore, the warm climate and infrequent snow occurrences render ΔSWE negligible, while ΔCWS has minimal impact. Consequently, for GWS estimation, these components are excluded from TWS, derived using average data from JPL and CSR, ensuring fairness in calculations through the subtraction of the GLDAS-SM component.

$$\Delta \text{GWS} = \Delta \text{TWS} - \Delta \text{SMS} \quad (2)$$

### 3.2. Gravity Anomaly (GA)

According to Newton's law of universal gravitation, the mass nearby affects the gravitational acceleration at a specific location. The gravitational acceleration at the Earth's surface changes in proportion to changes in an aquifer's mass brought about by processes such as recharge or discharge into surface water or wells. Even though this change is slight, it can be detected. In addition to groundwater-related variables, Earth tides, changes in barometric pressure, mass shifts brought on by volcanic activity, and other variables can all affect gravity measurements [63]. Most of these effects are either negligible or can be taken into account in groundwater studies.

In geodesy, gravity anomalies are used to define the figure of the Earth, notably the geoid (the equipotential surface of the Earth's gravity field that corresponds most closely to mean sea level). They are used in geodesy in three main areas: (1) to determine the anomalous potential $T$, the geoid's undulation $N$, and the vertical deflections, globally and locally [63]; (2) to determine the vertical crustal deformation by studying the variation of the gravitational field over time [64]; and (3) to adjust various geodetic readings, including leveling observations [65]. The GA or $\Delta g$ is expressed as Heiskanen and Moritz [63]:

$$\Delta g(r,\varphi,\lambda) = \frac{km}{r^2}\sum\nolimits_{n=2}^{\infty}(n-1)\left(\frac{a}{r}\right)^n\sum\nolimits_{m=0}^{n}\left(\overline{C}_{nm}^{*}\cos(m\lambda)+\overline{S}_{nm}\sin(m\lambda)\right)\overline{P}_{nm}(\cos\psi) \quad (3)$$

where $\Delta g$ is the gravity anomaly measured by mGal, $km$ is the geocentric gravitational constant of the earth, $r$ is the geocentric radius, $\varphi$, and $\psi$ are the geodetic and geocentric latitudes, $\lambda$ is the geodetic longitude, $a$ is the ellipsoidal semi-major axis radius, and $\overline{P}_{nm}(cos\psi)$ is the fully normalized associated Legendre function. $\overline{C}_{nm}^{*}$ and $\overline{S}_{nm}$ are the fully normalized spherical harmonic coefficients.

Figure 5 shows the average gravity anomaly during the period of the study in Arabian Peninsula in addition to the topography heights. Figure 5a displays the mean gravity anomaly from April 2002 to June 2023, and Figure 5b shows the topography in the same location, which provides a comprehensive view of the gravitational variations. In interpreting this figure, the heights of the topography in Figure 5b offer crucial context to the gravitational changes observed in Figure 5a. Gravity anomalies are influenced by the distribution of mass beneath the Earth's surface, and the topography in Figure 5b indicates elevations and depressions in the landscape.

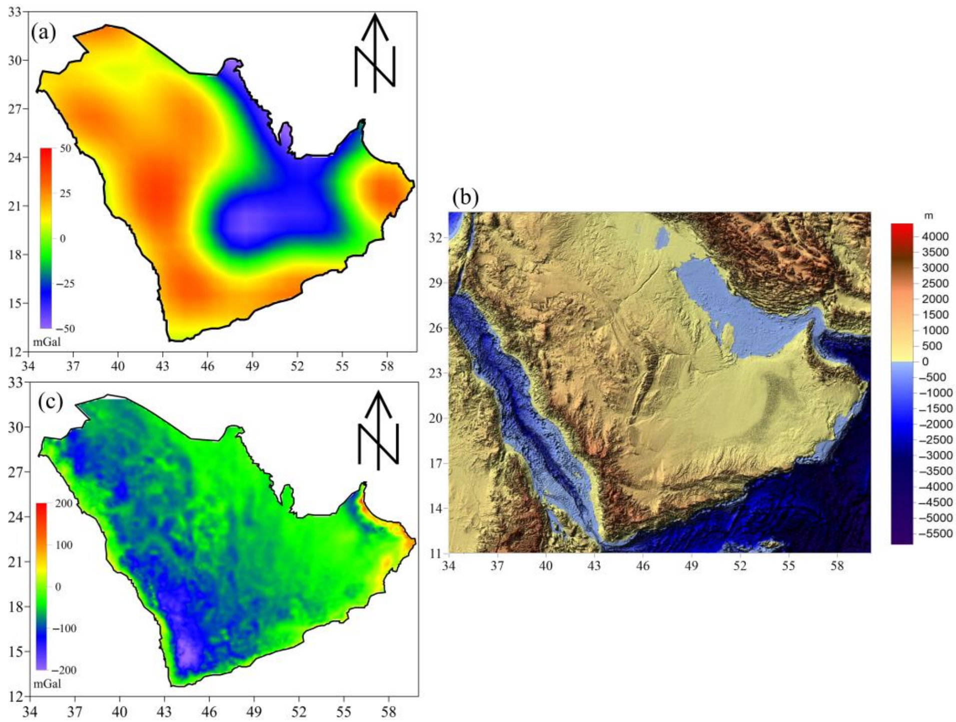


**Figure 5.** (**a**) The gravity anomaly mean from April 2002 to June 2023 (authors' calculation); (**b**) topography heights over the Arabian Peninsula (authors' calculation). (**c**) The Bouguer anomalies derived from the official Earth Gravitational Model (EGM2008) released by the National Geospatial Intelligence Agency (NGA).

Areas with higher topography in Figure 5b, such as mountains or elevated terrain, may exhibit corresponding anomalies in Figure 5a due to the increased mass concentration. Conversely, regions with lower topography could result in gravitational anomalies reflecting reduced mass beneath the surface. Localized features in the topography, like valleys or ridges, might correlate with distinctive patterns in the gravity anomaly, showcasing the gravitational impact of geological structures. Anomalies in Figure 5a might be linked to variations in subsurface mass, such as underground geological formations or changes in groundwater storage, which can be inferred by considering the heights and contours of the topography in Figure 5b.

In Figure 5c, a gravity anomaly represents deviations from the expected gravitational field due to variations in subsurface density. Positive anomalies indicate regions with higher-than-expected gravity, while negative anomalies suggest lower gravity. The Bouguer correction accounts for the gravitational effects of surface topography and near-surface masses (such as mountains or valleys). By subtracting the gravitational attraction of these masses, we obtain a more accurate representation of deeper subsurface anomalies. In the Arabian Peninsula, we observe positive Bouguer anomalies in areas like the Hadhramaut Basin in Yemen and the Rub' al Khali (Empty Quarter) desert, likely due to denser subsurface materials. Negative anomalies are also present, such as parts of the Red Sea and the Gulf of Aden. These gravity anomalies align with tectonic features like the Red Sea Rift, the Gulf of Aden Rift, the Arabian Shield, and the Zagros Mountains.

### *3.3. Seasonal AutoRegressive Integrated Moving Average Model (SARIMA)*

In this analysis, the SARIMA model was employed to capture and predict the temporal GWS in the Arabian Peninsula over the course of 255 months, from April 2002 to June 2023. The SARIMA model, an extension of the ARIMA model, proves to be a robust framework for time-series forecasting, especially in scenarios marked by discernible seasonal patterns [66]. Denoted as SARIMA (p, d, q) (P, D, Q), the model parameters include AutoregRessive (AR) order p, differencing order d, moving average order q, seasonal autoregressive order P, seasonal differencing order D, seasonal moving average order Q, and the seasonal period s. The SARIMA model begins its application with an exploration of the time-series data for inherent trends and seasonality. If necessary, differencing operations are employed to achieve stationarity. The core of the model involves the meticulous selection of optimal parameter values through the analysis of autocorrelation and partial autocorrelation functions. Following this, the dataset is partitioned into training and testing sets to facilitate model fitting and evaluation [67].

The training phase entails fitting the SARIMA model to the training data, employing statistical techniques to estimate the chosen parameters [68]. Validation of the model's performance occurs through the evaluation of key metrics, including correlation coefficients and mean squared error, using the testing dataset [69]. Once validated, the SARIMA model is poised for forecasting future values beyond the observed data [70]. Mathematically, the SARIMA forecasting equation can be expressed as follows:

$$\begin{gathered}\hat{y}_t = c + \varphi_1 y_{t-1} + \varphi_2 y_{t-2} + \ldots + \varphi_p y_{t-p} - \theta_1 \varepsilon_{t-1} - \theta_2 \varepsilon_{t-2} - \ldots - \theta_q \varepsilon_{t-q} \\ + \Phi_1 y_{t-s} + \Phi_2 y_{t-2s} + \ldots + \Phi_P y_{t-Ps} + \in_t\end{gathered} \tag{4}$$

where $\hat{y}_t$ represents the forecasted value, c is the constant term, $\varphi_i$ and $\theta_i$ are autoregressive and moving average coefficients, respectively, $\Phi_i$ is seasonal autoregressive coefficients, $y_{t-i}$ is past observations, $\varepsilon_{t-i}$ is past forecast errors, $s$ is the seasonal period, and $\in_t$ is the error term. This comprehensive methodology ensures that the SARIMA model is adeptly tailored to capture both short-term fluctuations and long-term seasonality, offering a reliable framework for forecasting within the context of the Arabian Peninsula's groundwater storage dynamics.

### *3.4. Multi-Linear Regression Analysis*

In multiple linear regression (MLR) analysis, the t-statistic plays a crucial role in evaluating the statistical significance of individual predictor variables within the model [71]. If $Y$ is the dependent variable, $\beta_0$ is the intercept term, $\beta_1,\ \beta_2,\ \ldots, \beta_k$ are the coefficients associated with the predictor variables, $X_1,\ X_2,\ \ldots, X_k$ are the predictor variables, and $\varepsilon$ is the error term, the MLR model using the equation:

$$Y = \beta_0 + \beta_1 X_1 + \beta_2 X_2 + \ldots + \beta_k X_k + \varepsilon \quad (5)$$

The primary objective of the t-test is to assess whether the estimated coefficient $\hat{\beta}_i$ of a predictor variable is significantly different from zero, implying a non-zero impact on the dependent variable. In the context of MLR, hypothesis testing is employed for each predictor variable using the t-statistic [72]. The null hypothesis ($H_0$) posits that the coefficient of the predictor variable is equal to zero, suggesting no effect. Conversely, the alternative hypothesis ($H_1$) asserts that the coefficient is not equal to zero, indicating a significant impact. The calculation of the t-statistic $t_i$ involves dividing the estimated coefficient by its standard error ($SE(\hat{\beta}_i)$):

$$t_i = \frac{\hat{\beta}_i}{SE(\hat{\beta}_i)} \quad (6)$$

A large absolute t-value, whether positive or negative, suggests that the predictor variable is likely to be statistically significant. In practical terms, a t-statistic far from zero indicates that the variable has a substantial impact on the dependent variable [73]. The degrees of freedom for the t-test in MLR are related to the sample size and the number of predictor variables. The significance level, often set to 0.05, determines the threshold for rejecting the null hypothesis. If the $p$-value associated with the t-statistic falls below this threshold, the null hypothesis is rejected, signifying statistical significance.

## 4. Results and Discussion

### *4.1. The GWS Effects on Gravity Anomaly*

In this study, a time-series comparison is conducted between GWS and GA. GWS is estimated using GRACE mascon data, while GA is estimated using GRACE SHCs data. Remarkably, both datasets demonstrate similar behavior, characterized by a consistent decline (Figure 6). Notably, there is a substantial decline observed from April 2002 to June 2023, with the GWS demonstrating a trend of $-4.59 \pm 0.84$ mm/year.

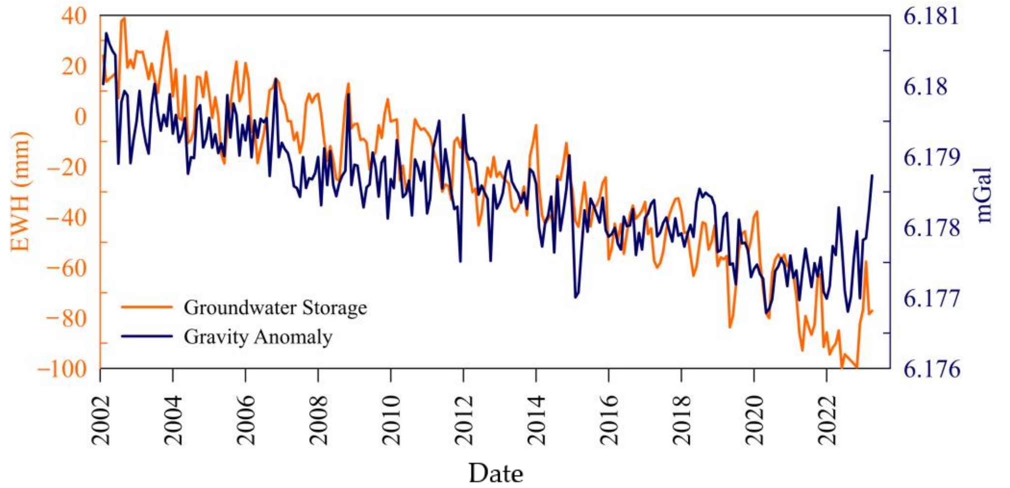


**Figure 6.** Time-series includes GWS and GA, which means that the left Y axis represents the GWS variation heights and the right Y axis represents the GA values (authors' calculation).

Figure 7 explores the temporal dynamics of GA and GWS within the AP. We conducted an extensive time-series analysis that involved decomposing the data into original, seasonal, and trend. The depiction of the original GA data in Figure 7(b1) unveils a nuanced temporal evolution. Throughout the investigation period, a gradual decrease in GA values is evident, signaling shifts in subsurface conditions. The variations in GA may be influenced by geological structures and hydrological processes, prompting a deeper inquiry into the specific factors contributing to these changes. Likewise, the original GWS data (Figure 7(a1)) mirror the behavior observed in GA. However, distinctive periods of deviation suggest a potential relationship between GWS dynamics and variations in GA. The observed drop in GWS during specific intervals aligns with decreases in GA, suggesting a potential linkage between these hydrogeological parameters.

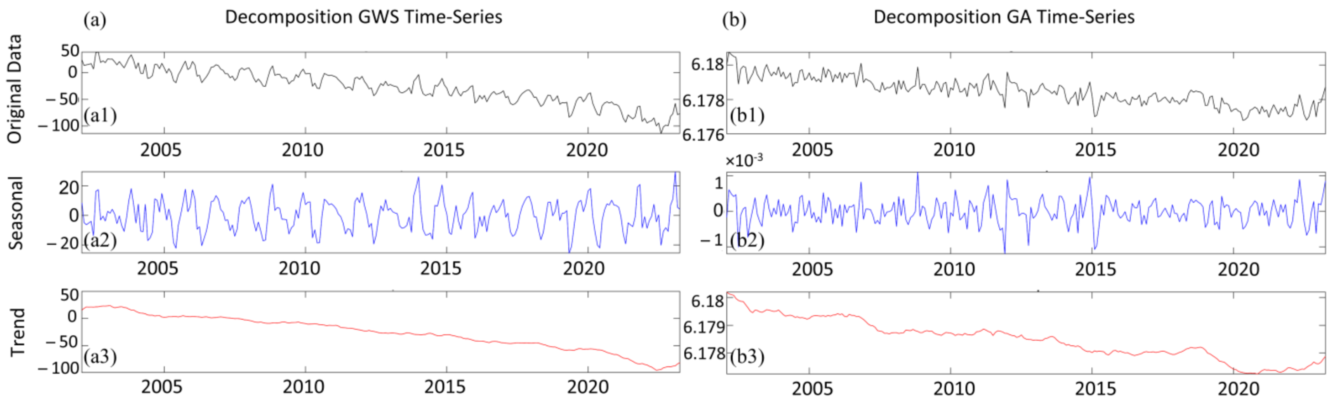


**Figure 7.** The time-series analysis decomposition of (**a**) GWS and (**b**) GA. For GWS, the decomposition comprises three subfigures: (**a1**) for the original data, (**a2**) for the seasonal component, and (**a3**) for the trend component. Similarly, the decomposition of GA includes three subfigures denoted as (**b1**) for the original data, (**b2**) for the seasonal component, and (**b3**) for the trend component (authors' calculation).

The seasonal component of GA (Figure 7(b1)) reveals cyclic patterns throughout the year, with peaks and troughs corresponding to distinct seasons. This seasonal influence is notably aligned with changes in precipitation and temperature, underscoring the sensitivity of GA to climatic conditions in the AP. Similarly, the GWS data (Figure 7(a2)) display analogous seasonal patterns, with fluctuations corresponding to different seasons. The temporal alignment of variations in GA and GWS underscores the interconnectedness of these parameters, reinforcing the idea that seasonal climatic factors play a pivotal role in shaping hydrogeological processes.

Examining the trend component, the downward trajectory of GA (Figure 7(b3)) suggests a sustained decrease in values over the study period. This long-term trend may be associated with regional hydrogeological changes, potentially linked to alterations in groundwater recharge. It captures short-term irregularities not explained by the seasonal and trend components. The GWS trend (Figure 7(a3)) closely mirrors the GA trend, further highlighting the potential correlation between these parameters. The synchronized downward trajectory implies that long-term changes in GA are closely tied to corresponding variations in groundwater storage. The trend exhibits short-term fluctuations deviating from the overall trend and seasonal patterns.

The comparative analysis of GA and GWS time-series in the AP unveils a complex relationship between these hydrogeological parameters. The alignment of seasonal variations, trends, and short-term anomalies emphasizes the interconnectedness of GA and GWS.

### *4.2. GWS Seasonal Analysis*

Groundwater storage in the AP exhibits a statistically significant decline over the entire study period. By using two types of GWS estimation, GRACE and WGHM, we estimated GWS up to 2019 and compared them. In addition, we estimated the GWS trend throughout all our periods of study. As shown in Figure 8 and Table 2, comparing the GWS trends for the time period from January 2003 to December 2019, the trend obtained from WGHM is approximately −3.30 ± 0.67 mm/year, which represents GWS depletion of 10.0 km$^3$/year, whereas the GRACE-derived trend is approximately −4.41 ± 0.81 mm/year, which represents GWS depletion of 13.36 km$^3$/year.

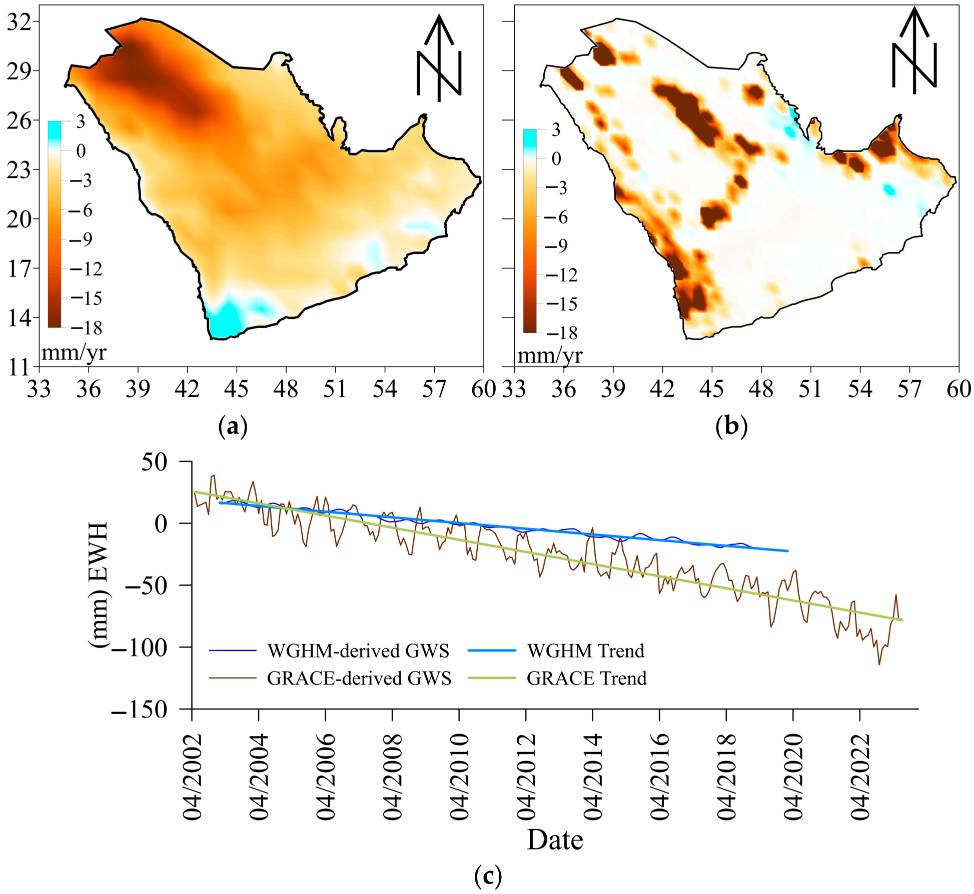


**Figure 8.** The GWS trend using GRACE and WGHM; (**a**) the GRACE-derived GWS trend from April 2002 to June 2023; (**b**) the WGHM-derived GWS trend from January 2003 to December 2019; (**c**) the GWS time-series using GRACE and WGHM (authors' calculation).

**Table 2.** The GWS trend over the AP were estimated using GRACE and WGHM (authors' calculation).

| GWS | GWS Trend (mm/Year) | | GWS Depletion (km$^3$/Year) 2002–2023 | Average Prec. (mm/Year) 2002–2023 | Average ET (mm/Year) 2002–2023 |
|---|---|---|---|---|---|
| | 2002–2019 | 2002–2023 | | | |
| GRACE-derived GWS | −4.41 ± 0.81 | −4.89 ± 0.86 | −14.82 ± 2.61 | 95.88 ± 0.50 | 80.88 ± 0.61 |
| WGHM-derived GWS | −3.30 ± 0.67 | — | | | |

Both time-series are highly correlated with each other; the correlation coefficient between both time-series is about 0.88. The GRACE-derived GWS trend over the period of study from April 2002 to June 2023 shows a significant declination about of −4.89 ± 0.86 mm/year, which represents −14.82 km$^3$/year depletion (Table 2). The GRACE and WGHM results demonstrate spatial domain similarity with strong signals using GRACE's behavior in GWS. The results show a negative trend throughout the entire area. The Arabian Peninsula is well known for its oil production, with an average annual production of 1.1 km$^3$/year (or 19–20 million barrels per day) in this region. This rate amounts to around 7.5% of the total depletion estimated by GRACE-derived GWS measurements (as shown in Table 2).

According to Figure 8a, the most stressed region is the north AP, and the depletion rate reaches about 17 mm/year in the An-Nafud desert and Hail region in Saudia Arabia. While the most wet region is south of AP in southwestern Yemen in Aden and Hudaydah cities, in addition to south parts of Oman country, these regions, according to our results in Figure 3b, show that most regions had precipitation in AP during the period of study. In the Arabian Peninsula, the WGHM does not smoothly capture changes in GWS within the spatial domain, unlike the GRACE-derived GWS. GRACE, utilizing satellite-based measurements, provides a broader-scale view of GWS changes, offering a more comprehensive spatial perspective. However, it is important to note that globally, the WGHM adequately captures spatial patterns of groundwater depletion [39,59]. However, the reliability of the GW variability modeled by WGHM depends strongly on optimal irrigation estimates and the corresponding GWS abstraction rates. Improved GWS variability and trends are obtained when assimilating GRACE-based TWSA into the models [74]. The discrepancies between the GRACE-derived GWS trends and those from WGHM can be attributed to the inherent differences in the methodologies and data sources of these two models for approximately three reasons: (1) Scale of Measurement: GRACE measures groundwater storage changes on a broader scale, utilizing satellite-based measurements that provide a more comprehensive spatial perspective. In contrast, WGHM is a model-based approach that relies on ground-based measurements and climatic data. This difference in scale might result in WGHM not capturing the changes in GWS as smoothly as GRACE. (2) Data Assimilation: The reliability of GW variability modeled by WGHM depends strongly on optimal irrigation estimates and the corresponding GWS abstraction rates. Any inaccuracies in these estimates could lead to discrepancies in the GWS trends derived from WGHM and GRACE. (3) Model Limitations: While WGHM has been found to adequately capture global spatial patterns of GW depletion, it might not be as effective in regions with complex hydrogeological characteristics or where data is sparse or unreliable.

### *4.3. Climate Factors Effect on GWS and GA*

The extensive use of GWS reflects the drought in this region. The Global Precipitation Climatology Centre Drought Index (GPCC-DI) assesses water supply anomalies based on long-term statistics. Combining the Standardized Precipitation Index (SPI-DWD) with adaptations from Deutscher Wetterdienst and the Standardized Precipitation Evapotranspiration Index (SPEI), it utilizes precipitation data from the GPCC and temperature data from NOAA's CPC. Available in various accumulation periods (1, 3, 6, 9, 12, 24, and 48 months) for diverse applications, the GPCC-DI has been issued monthly since January 2013 [75]. It is calculated on a regular grid with a $1^{\circ}$ spatial resolution.

In this analysis, monthly data were utilized to calculate the average, spanning from January 2013 to June 2023. Following the classification of GPCC-DI values, Lloyd-Hughes and Saunders [76], positive values indicate wet conditions, whereas negative values denote drought. The severity of drought or wetness increases progressively from mild (0 to $-1$ or 1) to moderate (up to $-1.5$ or 1.5), severe ($-1.5$ or 1.5 to $-2$ or 2), and extremely severe (above $-2$ or 2), respectively. The findings reveal that a significant portion of the Arabian Peninsula experiences extremely severe drought, particularly in the central region (refer to Figure 9). Conversely, areas of high elevation in the western and southern parts of the AP exhibit wet conditions (refer to Figures 9 and 5b).

One prominent factor contributing to the substantial depletion of groundwater in this region is its climatic conditions. The precipitation rate in the Arabian Peninsula (AP) is notably scarce when compared to the rate of evapotranspiration (ET). Monthly precipitation rates hover around a comparable magnitude to ET rates in AP, providing minimal opportunity for GWS replenishment. Figure 10 illustrates the sharp decline in the GWS time-series, juxtaposed with the bar chart depicting the average monthly precipitation and ET.

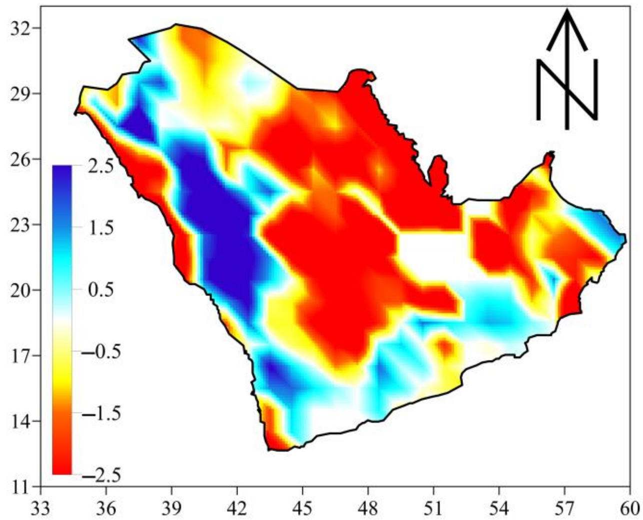


**Figure 9.** The average monthly drought index for the time frame between January 2013 and June 2023, using monthly GPCC data. The drought is depicted in colors ranging from yellow to red, with the severity of the drought increasing from mild (0 to −1) to moderate (up to −1.5), severe (−1.5 to −2), and extremely severe (below −2). Conversely, the wet is represented by a range of blue hues, with the level of wetness increasing from mild (0 to 1) to moderate (up to 1.5), severe (1.5 to 2), and extremely severe (above 2) (authors' calculation).

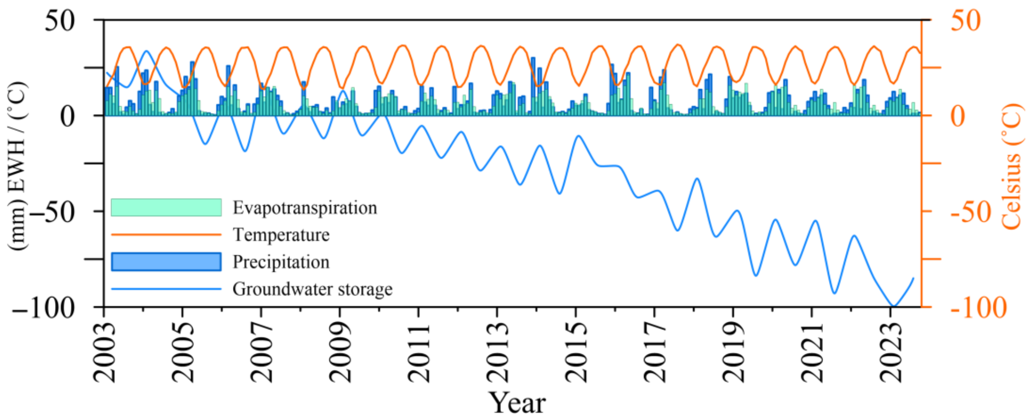


**Figure 10.** Comprehensive analysis of GWS trends and meteorological factors in the AP. This figure comprises a time-series of GRACE-derived GWS, the mean temperature, and a bar chart depicting Pr and ET (authors' calculation).

The monthly precipitation and ET exhibit considerable variability, fluctuating from approximately zero to about 30 mm, with an average of 7.99 mm for monthly precipitation and 6.74 mm for ET (Figure 10). This rate is classified as relatively low compared to global averages. Given these rates and the equilibrium between precipitation and ET, compounded by the region's high temperatures (as discussed in Section 2.1) and the substantial water demand for a population exceeding 97 million people (refer to Table 1), the GWS undergoes a significant decline. This depletion of GWS further influences the equilibrium of gravitational forces in the region, contributing to a notable shift in the gravity balance. The intricate interplay between these climatic, hydrological, and demographic factors underscores the challenges faced by the Arabian Peninsula in sustaining groundwater resources amidst escalating demand and unfavorable climate conditions.

Due to a better understanding of this relationship, we employed a multiple linear regression model to investigate the relationship between GA, with GWS, precipitation, and ET (Figure 11). The main two components', GWS and GA, trends show the same declination direction. Therefore, the model demonstrated a significant fit, explaining a substantial proportion of the variance in GA, as indicated by the high R-squared value of 0.8061.

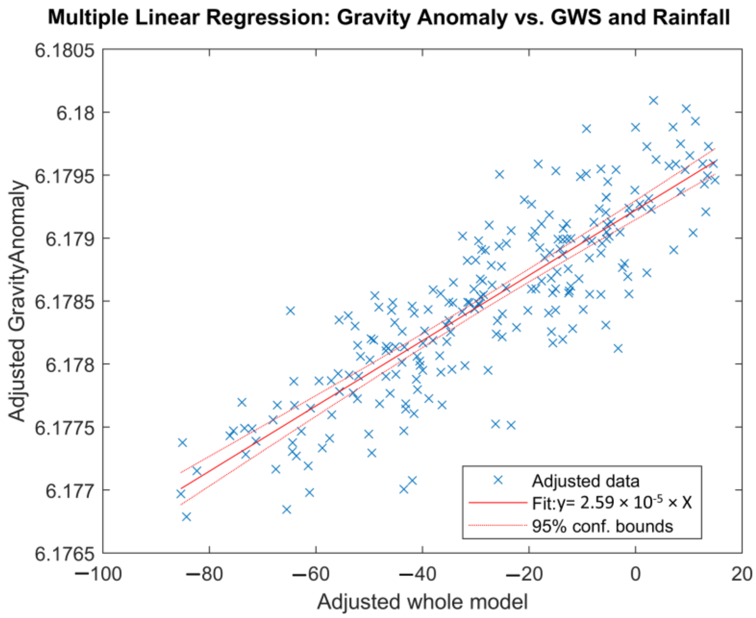


**Figure 11.** Multi-linear regression for GA with GWS, precipitation, and ET (authors' calculation).

The regression coefficients indicated that both GWS and precipitation and ET were significant predictors of GA. For instance, for every unit increase in GWS, the gravity anomaly increased by $2.32 \times 10^{-5}$, assuming rainfall is held constant. Similarly, for every unit increase in precipitation, the GA decreased by $1.16 \times 10^{-5}$, assuming GWS is held constant. These relationships were statistically significant at the 0.05 level ($p$-values: $2.47 \times 10^{-65}$, for GWS, $4.09 \times 10^{-5}$ for precipitation and 0.0097 for ET). Residual analysis revealed that the assumptions of the regression model were adequately met. The residuals were randomly distributed around zero when plotted against the predicted values, suggesting that the model provided a good fit to the data.

Correlation Analysis

The results of the correlation analysis between GA with GWS and rainfall provide valuable insights into the hydrogeological dynamics of the AP during the period of study (Figure 12). The correlation coefficients reveal a notably strong correlation of 0.8 between GA and GWS. This substantial correlation suggests a robust and consistent relationship between GA values and variations in GWS levels. The high positive correlation implies that changes in GWS contribute significantly to the observed variations in GA. This finding aligns with expectations, as fluctuations in groundwater levels can influence the density distribution in the subsurface, consequently impacting GA measurements.

Contrastingly, the correlation between GA and rainfall is observed to be weak. The coefficient of correlation, as evidenced by the scatter plot, suggests a lack of a strong linear relationship between GA and rainfall in the studied period (as discussed earlier in Figure 10). This outcome underscores that precipitation patterns alone may not be the dominant driver of gravity anomaly changes over the analyzed timeframe.

Consequently, the correlation analysis indicates a robust connection between gravity anomalies and GWS in the AP, affirming the sensitivity of GA to changes in groundwater levels. Conversely, the weak correlation with rainfall emphasizes the need to explore additional factors influencing GA dynamics in the region. These findings contribute valuable insights to the understanding of hydrogeological processes in the AP and underscore the complex interplay of environmental variables influencing GA variations.

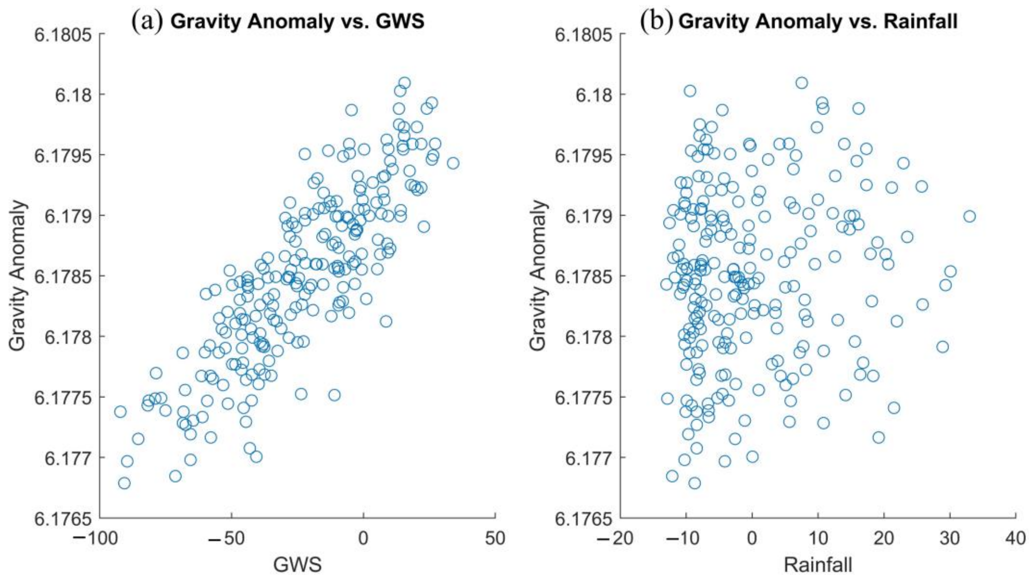


**Figure 12.** A scattered chart represents a correlation analysis for (**a**) GA and GWS and (**b**) GA and precipitation (authors' calculation).

### *4.4. GWS Prediction*

In this study, a SARIMA model was utilized to predict GWS over the Arabian Peninsula, spanning 255 months from April 2002 to June 2023. The groundwater storage forecasting employed an ARIMA (4,0,2) model with SARIMA, featuring an autoregressive (AR) component covering lags 1 to 4, a moving average (MA) component at lags 1 and 2, and seasonality introduced through seasonal AR terms at multiples of 12 (SAR) up to lag 48. The model effectively captures both short-term and long-term dependencies within the GWS time-series data. Statistical tests on the parameter estimates elucidate the significance of each component; specifically, the constant term demonstrates statistical significance ($p$-value < 0.05), suggesting a meaningful impact on groundwater storage. Likewise, multiple autoregressive and seasonal coefficients exhibit statistical significance, underscoring their relevance in elucidating variations in the GWS time-series. In our study, all $p$-values for coefficients are below 0.05, indicating the statistical significance of each corresponding coefficient.

Figure 13 shows the GWS time-series divided into three parts training data, testing data, and predicted data using the SARIMA model. The SARIMA model was applied to forecast GWS for an additional 120 months, extending the prediction period to mid-2033 beyond the initial 255-month observation span. Utilizing 80% of the data (204 months) for training and reserving the remaining 20% (51 months) for testing, the robust correlation coefficient of 0.94 between the test and predicted data over the 51-month test period underscores the reliability of the predictive insights.

Comparatively, when juxtaposed with the GRACE-derived GWS trend of $-4.89 \pm 0.86$ mm/year, the forecasted trend for the upcoming 120 months manifests as $-4.79 \pm 0.79$ mm/year. This observation implies a noteworthy overall depletion trend of approximately $-5.15 \pm 0.94$ mm/year (equivalent to $\approx$15.97 km$^3$/year) across the expansive Arabian Peninsula. While interpreting these results, due consideration should be given to the inherent uncertainties associated with long-term forecasting, coupled with the dynamic and intricate nature of groundwater systems in this geographically diverse region.

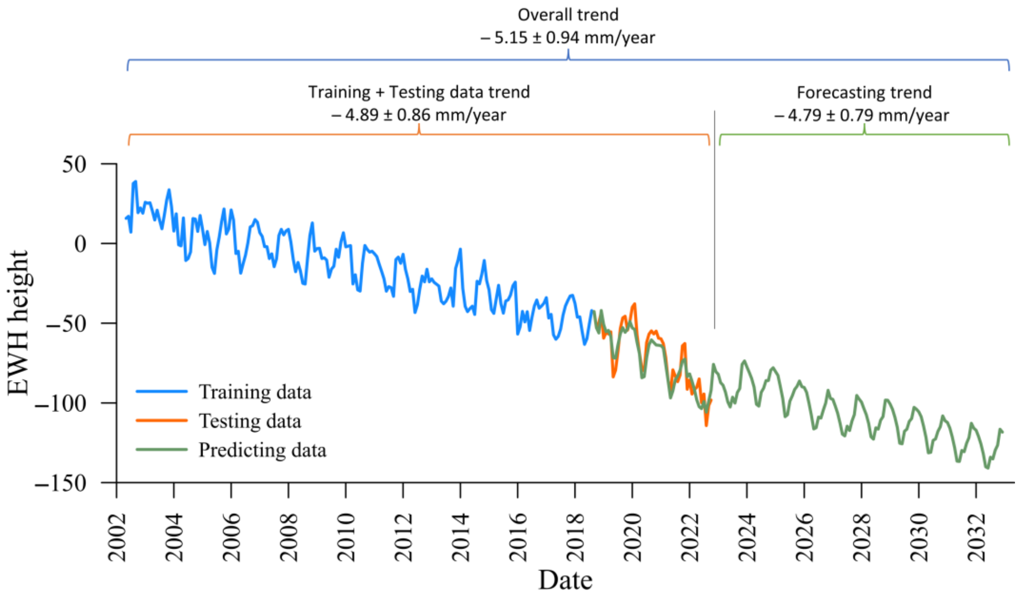


**Figure 13.** The GWS time-series forecasted by the SARIMA model, spanning from April 2002 to mid-2033. The graph features three distinct lines: the blue line represents the training data, the orange line signifies the testing data, and the green line depicts the predicted GWS values (authors' calculation).

Given the significant depletion of GWS, it is crucial to study this depletion in the AP. Understanding its impact on gravity stability and, consequently, crust stability, is essential for the future. To mitigate groundwater depletion, we recommend several strategies: enforce stricter water management policies; explore artificial recharge methods (such as injecting treated wastewater or excess surface water into aquifers); invest in desalination plants, promote sustainable agriculture practices; and raise public awareness about water conservation. Integrated water resource management plans should consider both surface water and groundwater, tailored to the unique hydrogeological characteristics and socio-economic context of the region.

## 5. Conclusions

In conclusion, this study investigated the intricate relationships between groundwater storage and gravity changes in the Arabian Peninsula. To study GWS behavior, we integrate datasets from GRACE and GLDAS, as well as climate factors such as precipitation, temperature, and evaporation. The analysis reveals a deeply concerning trend of extremely severe drought due to low precipitation, with an average precipitation of $95.88 \pm 0.50$ mm/year and average evaporation of $80.88 \pm 0.61$ mm/year during the study period, attributed to an average temperature of 26.5 °C. This drought peak is particularly severe in the Arabian Peninsula's central region, posing a significant challenge to groundwater replenishment. In contrast, the southwest had humid conditions. The time-series analysis revealed a significant decline in GWS from April 2002 to June 2023, with an observed rate of approximately $-4.59 \pm 0.84$ mm/year, according to GRACE observations. Groundwater volume decreased by $-14.82 \pm 2.61$ km$^3$/year, highlighting its impact on the gravity field. The WGHM hydrological model predicted a groundwater decline of $-3.30 \pm 0.67$ mm/year from 2003 to 2019. Temporal analysis of GWS and gravity anomalies (GAs) reveals a parallel decrease, which explains the region's negative gravitational changes. Climate factor analysis indicates a scenario of severe drought (>2.5) in the Arabian Peninsula, particularly in the central region, consistent with the GPCC-DI, and precipitation scarcity was evident. The SARIMA model predicts a $-5.15 \pm 0.94$ mm/year depletion trend over the next 120 months until June 2033, surpassing previous analyses. A multiple linear regression model was used to investigate the interaction of GWS, GA, and climatic factors. The model shows that GWS, precipitation, and evaporation have a significant influence on GA, accounting for

80.61% of the variance. The strong correlation (0.8) between GWS and GA demonstrates the importance of GWS in shaping gravitational variations in the region.

**Author Contributions:** Conceptualization, H.A.M.; methodology, H.A.M. and J.J.; software, H.A.M.; validation, H.A.M., J.J., H.A.A.-E. and W.S.; writing—original draft preparation, H.A.M.; writing—review and editing, J.J. and W.S.; visualization, W.S. and H.A.A.-E.; supervision, W.S. All authors have read and agreed to the published version of the manuscript.

**Funding:** This research was funded by the National Natural Science Foundations of China (No. 41721003, 42030105, 41874023) and the Fundamental Research Funds for the Central Universities. In addition, the Open Fund of Wuhan Gravitation and Solid Earth Tides National Observation and Research Station (WHYWZ202202).

**Data Availability Statement:** The data presented in this study are available on request from the corresponding author and/or on the corresponding websites in the Acknowledgment section. CSR-mascon data can be downloaded from "https://www.csr.utexas.edu/grace/RL06_mascons.html (accessed on 2 January 2024)", GRACE CSR-SHCs "ftp:/isdcftp.gfz-potsdam.de/grace/Level-2/CSR/RL06/ (accessed on 2 January 2024)", GRACE-FO CSR-SHCs data can be downloaded from "ftp:/isdcftp.gfz-potsdam.de/grace-fo/Level-2/CSR/RL06/ (accessed on 2 January 2024)", GPCC drought index data are available at "http://dx.doi.org/10.5676/DWD_GPCC/DI_M_100 (accessed on 16 December 2023)".

**Acknowledgments:** The authors extend their gratitude to the Supercomputing Center of Wuhan University for generously providing access to their supercomputing system, which was instrumental in conducting the numerical calculations for this research.

**Conflicts of Interest:** The authors declare no conflicts of interest.

## References

1. Hunt, C.E. *Thirsty Planet: Strategies for Sustainable Water Management*; Academic Foundation: Ahmedabad, India, 2007.
2. Eyvaz, M.; Wan, Z.; Ahmad, S.; Wan, R. *Sustainable Development on Water Resources Management, Policy and Governance in a Changing World*; Frontiers Media SA: Lausanne, Switzerland, 2023. [CrossRef]
3. Shahin, M. *Water Resources and Hydrometeorology of the Arab Region*; Springer Science & Business Media: New York, NY, USA, 2007; Volume 59.
4. Tian, Y.; Zheng, Y.; Wu, B.; Wu, X.; Liu, J.; Zheng, C. Modeling surface water-groundwater interaction in arid and semi-arid regions with intensive agriculture. *Environ. Model. Softw.* **2015**, *63*, 170–184. [CrossRef]
5. Sherif, M.; Sefelnasr, A.; Al Rashed, M.; Alshamsi, D.; Zaidi, F.K.; Alghafli, K.; Baig, F.; Al-Turbak, A.; Alfaifi, H.; Loni, O.A. A review of managed aquifer recharge potential in the Middle East and North Africa Region with examples from the Kingdom of Saudi Arabia and the United Arab Emirates. *Water* **2023**, *15*, 742. [CrossRef]
6. Bahri, A. Water reuse in Middle Eastern and North African countries. In *Water Reuse: An International Survey of Current PRACTICE, Issues and Needs*; IWA Publishing: London, UK, 2008; pp. 27–47.
7. Khouri, J.; AUDrouby, A.; Gedeon, R.; Salih, A. *Groundwater Protection in the Arab Region*; IHP: Paris, France, 1995.
8. Sherif, M.; Liaqat, M.U.; Baig, F.; Al-Rashed, M. Water resources availability, sustainability and challenges in the GCC countries: An overview. *Heliyon* **2023**, *9*, e20543. [CrossRef]
9. Dawoud, M.A. Water Scarcity in the GCC Countries: Challenges and Opportunities. In *GRC Research Papers, in GRC Research Papers*; Gulf Research Center: Geneva, Switzerland, 2007.
10. Dolatyar, M.; Gray, T.S.; Dolatyar, M.; Gray, T.S. Water Politics in the Arabian Peninsula. In *Water Politics in the Middle East: A Context for Conflict or Co-Operation?* Springer: Berlin/Heidelberg, Germany, 2000; pp. 164–205. [CrossRef]
11. World Bank. *A Water Sector Assessment Report on the Countries of the Cooperation Council of the Arab States of the Gulf*; World Bank: Washington, DC, USA, 2005.
12. Wouters, B.; Bonin, J.A.; Chambers, D.P.; Riva, R.E.; Sasgen, I.; Wahr, J. GRACE, time-varying gravity, Earth system dynamics and climate change. *Rep. Prog. Phys.* **2014**, *77*, 116801. [CrossRef]
13. Chen, J. Satellite gravimetry and mass transport in the earth system. *Geod. Geodyn.* **2019**, *10*, 402–415. [CrossRef]
14. Gehman, C.L.; Harry, D.L.; Sanford, W.E.; Stednick, J.D.; Beckman, N.A. Estimating specific yield and storage change in an unconfined aquifer using temporal gravity surveys. *Water Resour. Res.* **2009**, *45*, W00D21. [CrossRef]
15. Al-Rashed, M.F.; Sherif, M.M. Water resources in the GCC countries: An overview. *Water Resour. Manag.* **2000**, *14*, 59–75. [CrossRef]
16. Siebert, S.; Burke, J.; Faures, J.-M.; Frenken, K.; Hoogeveen, J.; Döll, P.; Portmann, F.T. Groundwater use for irrigation–a global inventory. *Hydrol. Earth Syst. Sci.* **2010**, *14*, 1863–1880. [CrossRef]

17. Droogers, P.; Immerzeel, W.; Terink, W.; Hoogeveen, J.; Bierkens, M.; Van Beek, L.; Debele, B. Water resources trends in Middle East and North Africa towards 2050. *Hydrol. Earth Syst. Sci.* **2012**, *16*, 3101–3114. [CrossRef]
18. Odhiambo, G.O. Water scarcity in the Arabian Peninsula and socio-economic implications. *Appl. Water Sci.* **2017**, *7*, 2479–2492. [CrossRef]
19. Tashtush, F.M.; Al-Zubari, W.K.; Al-Haddad, A.S. The Use of Non-Conventional Water Resources in Agriculture in the Gulf Cooperation Council Countries: Key Challenges and Opportunities for the Use of Treated Wastewater. In *Biosaline Agriculture as a Climate Change Adaptation for Food Security*; Springer: Berlin/Heidelberg, Germany, 2023; pp. 285–322. [CrossRef]
20. FAO. *Review of World Water Resources by Country*; Water Reports No. 23; Food & Agriculture Organization of the UN (FAO): Rome, Italy, 2003.
21. UN-Water (Ed.) *Global Annual Assessment of Sanitation and Drinking-Water (GlAAS) 2012 Report: The Challenge of Extending and Sustaining Services*; UN: New York, NY, USA, 2012.
22. Ojha, R.; Ramadas, M.; Govindaraju, R.S. Current and future challenges in groundwater. I: Modeling and management of resources. *J. Hydrol. Eng.* **2015**, *20*, A4014007. [CrossRef]
23. Green, T.R.; Taniguchi, M.; Kooi, H.; Gurdak, J.J.; Allen, D.M.; Hiscock, K.M.; Treidel, H.; Aureli, A. Beneath the surface of global change: Impacts of climate change on groundwater. *J. Hydrol.* **2011**, *405*, 532–560. [CrossRef]
24. Tapley, B.D.; Bettadpur, S.; Ries, J.C.; Thompson, P.F.; Watkins, M.M. GRACE measurements of mass variability in the Earth system. *Science* **2004**, *305*, 503–505. [CrossRef]
25. Kirschner, M.; Massmann, F.-H.; Steinhoff, M. GRACE. In *Distributed Space Missions for Earth System Monitoring*; Springer: Berlin/Heidelberg, Germany, 2012; pp. 547–574. [CrossRef]
26. Frappart, F.; Ramillien, G. Monitoring groundwater storage changes using the Gravity Recovery and Climate Experiment (GRACE) satellite mission: A review. *Remote Sens.* **2018**, *10*, 829. [CrossRef]
27. Rodell, M. *11 Satellite Gravimetry. Remote Sensing of Drought: Innovative Monitoring Approaches*; CRC Press: Boca Raton, FL, USA, 2012; p. 261.
28. Seeber, G. *Satellite Geodesy*; Walter de gruyter: Berlin, Germany, 2003. [CrossRef]
29. Chen, J.; Famigliett, J.S.; Scanlon, B.R.; Rodell, M. Groundwater storage changes: Present status from GRACE observations. In *Remote Sensing and Water Resources*; Springer: Berlin/Heidelberg, Germany, 2016; pp. 207–227. [CrossRef]
30. Mohasseb, H.A.; Shen, W.; Jiao, J.; Wu, Q. Groundwater Storage Variations in the Main Karoo Aquifer Estimated Using GRACE and GPS. *Water* **2023**, *15*, 3675. [CrossRef]
31. Abd-Elmotaal, H.A.; Makhloof, A.; Hassan, A.A.; Mohasseb, H. Preliminary results on the estimation of ground water in Africa using GRACE and hydrological models. In Proceedings of the International Symposium on Gravity, Geoid and Height Systems 2016: Proceedings Organized by IAG Commission 2 and the International Gravity Field Service, Thessaloniki, Greece, 19–23 September 2016; pp. 217–226.
32. Richey, A.S.; Thomas, B.F.; Lo, M.H.; Reager, J.T.; Famiglietti, J.S.; Voss, K.; Swenson, S.; Rodell, M. Quantifying renewable groundwater stress with GRACE. *Water Resour. Res.* **2015**, *51*, 5217–5238. [CrossRef]
33. Bhanja, S.N.; Mukherjee, A.; Saha, D.; Velicogna, I.; Famiglietti, J.S. Validation of GRACE based groundwater storage anomaly using in-situ groundwater level measurements in India. *J. Hydrol.* **2016**, *543*, 729–738. [CrossRef]
34. Van der Gun, J. *Large Aquifer Systems Around the World*; The Groundwater Project; University of Guelph: Guelph, ON, Canada, 2022. [CrossRef]
35. Mohamed, A.; Alarifi, S.S.; Mohammed, M.A. Geophysical monitoring of the groundwater resources in the Southern Arabian Peninsula using satellite gravity data. *Alex. Eng. J.* **2024**, *86*, 311–326. [CrossRef]
36. Wehbe, Y.; Temimi, M. A remote sensing-based assessment of water resources in the Arabian Peninsula. *Remote Sens.* **2021**, *13*, 247. [CrossRef]
37. Alghafli, K.; Shi, X.; Sloan, W.; Shamsudduha, M.; Tang, Q.; Sefelnasr, A.; Ebraheem, A.A. Groundwater recharge estimation using in-situ and GRACE observations in the eastern region of the United Arab Emirates. *Sci. Total Environ.* **2023**, *867*, 161489. [CrossRef]
38. Fallatah, O.A.; Ahmed, M.; Save, H.; Akanda, A.S. Quantifying temporal variations in water resources of a vulnerable middle eastern transboundary aquifer system. *Hydrol. Process.* **2017**, *31*, 4081–4091. [CrossRef]
39. Döll, P.; Müller Schmied, H.; Schuh, C.; Portmann, F.T.; Eicker, A. Global-scale assessment of groundwater depletion and related groundwater abstractions: Combining hydrological modeling with information from well observations and GRACE satellites. *Water Resour. Res.* **2014**, *50*, 5698–5720. [CrossRef]
40. Mohamed, A.; Abdelrahman, K.; Abdelrady, A. Application of time-variable gravity to groundwater storage fluctuations in Saudi Arabia. *Front. Earth Sci.* **2022**, *10*, 873352. [CrossRef]
41. Fallatah, O.A. Groundwater quality patterns and spatiotemporal change in depletion in the regions of the Arabian Shield and Arabian Shelf. *Arab. J. Sci. Eng.* **2020**, *45*, 341–350. [CrossRef]
42. Agarwal, V.; Kumar, A.; Gomes, R.L.; Marsh, S. Monitoring of Ground Movement and Groundwater Changes in London Using InSAR and GRACE. *Appl. Sci.* **2020**, *10*, 8599. [CrossRef]
43. Khanna, P.; Petrovic, A.; Ramdani, A.I.; Homewood, P.; Mettraux, M.; Vahrenkamp, V. Mid-Holocene to present circum-Arabian sea level database: Investigating future coastal ocean inundation risk along the Arabian plate shorelines. *Quat. Sci. Rev.* **2021**, *261*, 106959. [CrossRef]

44. FAO. *FAO's Information System on Water and Agriculture (AQUASTAT)*; FAO: Rome, Italy, 2007.
45. UNESCO. *Water in a Changing World*; UNESCO: Paris, France, 2009.
46. Al-Eshlah, A.; Al-Rubaidi, H.; Al-Sabri, A. Agriculture's contribution to solving the water crisis. In Proceedings of the National Conference for the Management and Development of Water Resources in Yemen organized by the Ministry of Agriculture and Irrigation in January, Sana'a, Yemen, 15–17 January 2011.
47. AlSarmi, S.; Washington, R. Recent observed climate change over the Arabian Peninsula. *J. Geophys. Res. Atmos.* **2011**, *116*, D11109. [CrossRef]
48. Kornfeld, R.P.; Arnold, B.W.; Gross, M.A.; Dahya, N.T.; Klipstein, W.M.; Gath, P.F.; Bettadpur, S. GRACE-FO: The gravity recovery and climate experiment follow-on mission. *J. Spacecr. Rocket.* **2019**, *56*, 931–951. [CrossRef]
49. Li, Z.; Zhang, Z.; Wang, H. On Tide Aliasing in GRACE Time-Variable Gravity Observations. *Remote Sens.* **2022**, *14*, 5403. [CrossRef]
50. Sun, Z.; Long, D.; Yang, W.; Li, X.; Pan, Y. Reconstruction of GRACE data on changes in total water storage over the global land surface and 60 basins. *Water Resour. Res.* **2020**, *56*, e2019WR026250. [CrossRef]
51. Chen, J.; Tapley, B.; Tamisiea, M.E.; Save, H.; Wilson, C.; Bettadpur, S.; Seo, K.W. Error Assessment of GRACE and GRACE Follow-On Mass Change. *J. Geophys. Res. Solid Earth* **2021**, *126*, e2021JB022124. [CrossRef]
52. Swenson, S.; Chambers, D.; Wahr, J. Estimating geocenter variations from a combination of GRACE and ocean model output. *J. Geophys. Res. Solid Earth* **2008**, *113*, B08410. [CrossRef]
53. Swenson, S.; Wahr, J. Post-processing removal of correlated errors in GRACE data. *Geophys. Res. Lett.* **2006**, *33*, L08402. [CrossRef]
54. Rodell, M.; Houser, P.R.; Jambor, U.; Gottschalck, J.; Mitchell, K.; Meng, C.-J.; Arsenault, K.; Cosgrove, B.; Radakovich, J.; Bosilovich, M.; et al. The Global Land Data Assimilation System. *Bull. Am. Meteorol. Soc.* **2004**, *85*, 381–394. [CrossRef]
55. Rui, H.; Beaudoing, H.; Loeser, C. *README Document for NASA GLDAS Version 2 Data Products*; Goddart Earth Sciences Data and Information Services Center (GES DISC): Greenbelt, MD, USA, 2018.
56. Beaudoing, H.; Rodell, M. *NASA/Gsfc/Hsl. GLDAS Noah Land Surface Model L*; Goddard Earth Sciences Data and Information Services Center (GES DISC): Greenbelt, MD, USA, 2020; Volume 4, p. 3. [CrossRef]
57. Döll, P.; Fiedler, K. Global-scale modeling of groundwater recharge. *Hydrol. Earth Syst. Sci.* **2008**, *12*, 863–885. [CrossRef]
58. Döll, P.; Kaspar, F.; Lehner, B. A global hydrological model for deriving water availability indicators: Model tuning and validation. *J. Hydrol.* **2003**, *270*, 105–134. [CrossRef]
59. Müller Schmied, H.; Cáceres, D.; Eisner, S.; Flörke, M.; Herbert, C.; Niemann, C.; Peiris, T.A.; Popat, E.; Portmann, F.T.; Reinecke, R. The global water resources and use model WaterGAP v2. 2d: Model description and evaluation. *Geosci. Model Dev.* **2021**, *14*, 1037–1079. [CrossRef]
60. Gu, G.; Adler, R.F. Observed variability and trends in global precipitation during 1979–2020. *Clim. Dyn.* **2022**, *61*, 131–150. [CrossRef]
61. Efon, E.; Ngongang, R.D.; Meukaleuni, C.; Wandjie, B.; Zebaze, S.; Lenouo, A.; Valipour, M. Monthly, Seasonal, and Annual Variations of Precipitation and Runoff Over West and Central Africa Using Remote Sensing and Climate Reanalysis. *Earth Syst. Environ.* **2022**, *7*, 67–82. [CrossRef]
62. Seraphin, P.; Gonçalvès, J.; Hamelin, B.; Stieglitz, T.; Deschamps, P. Influence of intensive agriculture and geological heterogeneity on the recharge of an arid aquifer system (Saq–Ram, Arabian Peninsula) inferred from GRACE data. *Hydrol. Earth Syst. Sci.* **2022**, *26*, 5757–5771. [CrossRef]
63. Heiskanen, W.A.; Moritz, H. *Physical Geodesy*; Book on physical geodesy covering potential theory, gravity fields, gravimetric and astrogeodetic methods, statistical analysis, etc.; Springer: New York, NY, USA, 1967. [CrossRef]
64. Vanicek, P.; Krakiwsky, E.J. *Geodesy: The Concepts*; Elsevier: Amsterdam, The Netherlands, 2015. [CrossRef]
65. Tscherning, C. Determination of sea surface topography from satellite radar altimetry [ocean geoid, ocean circulation, altimeter]. In Proceedings of the Conference on Satellite Based Navigation and Remote Sensing of the Sea, Copenhagen, Denmark, 4 March 1980.
66. Prista, N.; Diawara, N.; Costa, M.J.; Jones, C.M. Use of SARIMA models to assess data-poor fisheries: A case study with a sciaenid fishery off Portugal. *Fish. Bull.* **2011**, *109*, 170–185.
67. Karim, A.A.; Pardede, E.; Mann, S. A Model Selection Approach for Time Series Forecasting: Incorporating Google Trends Data in Australian Macro Indicators. *Entropy* **2023**, *25*, 1144. [CrossRef]
68. Khashei, M.; Bijari, M.; Hejazi, S.R. Combining seasonal ARIMA models with computational intelligence techniques for time series forecasting. *Soft Comput.* **2012**, *16*, 1091–1105. [CrossRef]
69. Sirisha, U.M.; Belavagi, M.C.; Attigeri, G. Profit prediction using Arima, Sarima and LSTM models in time series forecasting: A Comparison. *IEEE Access* **2022**, *10*, 124715–124727. [CrossRef]
70. Samal, K.K.R.; Babu, K.S.; Das, S.K.; Acharaya, A. Time series based air pollution forecasting using SARIMA and prophet model. In Proceedings of the 2019 International Conference on Information Technology and Computer Communications, Singapore, 16–18 August 2019; pp. 80–85.
71. Sun, A.Y.; Scanlon, B.R.; Save, H.; Rateb, A. Reconstruction of GRACE total water storage through automated machine learning. *Water Resour. Res.* **2021**, *57*, e2020WR028666. [CrossRef]
72. Dhulipala, S.; Patil, G.R. Freight production of agricultural commodities in India using multiple linear regression and generalized additive modelling. *Transp. Policy* **2020**, *97*, 245–258. [CrossRef]

73. Konasani, V.R.; Kadre, S.; Konasani, V.R.; Kadre, S. Multiple regression analysis. In *Practical Business Analytics Using SAS: A Hands-on Guide*; Springer: Berlin/Heidelberg, Germany, 2015; pp. 351–399. [CrossRef]
74. Schumacher, M.; Forootan, E.; van Dijk, A.I.; Schmied, H.M.; Crosbie, R.S.; Kusche, J.; Döll, P. Improving drought simulations within the Murray-Darling Basin by combined calibration/assimilation of GRACE data into the WaterGAP Global Hydrology Model. *Remote Sens. Environ.* **2018**, *204*, 212–228. [CrossRef]
75. Ziese, M.; Schneider, U.; Meyer-Christoffer, A.; Schamm, K.; Vido, J.; Finger, P.; Bissolli, P.; Pietzsch, S.; Becker, A. The GPCC Drought Index–a new, combined and gridded global drought index. *Earth Syst. Sci. Data* **2014**, *6*, 285–295. [CrossRef]
76. Lloyd-Hughes, B.; Saunders, M.A. A drought climatology for Europe. *Int. J. Climatol. A J. R. Meteorol. Soc.* **2002**, *22*, 1571–1592. [CrossRef]